


# Generalized threshold of longitudinal multibunch instability in synchrotrons

Ivan Karpov  and Elena Shaposhnikova  
*CERN, CH 1211 Geneva 23, Switzerland*

 (Received 12 September 2023; accepted 6 June 2024; published 8 July 2024)

Beam stability is a crucial requirement for all particle accelerators. Coupled-bunch instability (CBI) is driven by beam interaction with narrowband impedance of the resonant accelerator components. Loss of Landau damping (LLD) for a single bunch is mainly determined by broadband impedance and can lead to undamped bunch oscillations. For the first time, we solve numerically the longitudinal stability problem in a self-consistent way for a general case of two impedance types and propose a simple analytical criterion describing how the obtained LLD and CBI thresholds are combined. We demonstrate that LLD can modify the CBI mechanism and reduce the instability threshold even below the LLD threshold. These findings allow the existing beam observations in CERN Super Proton Synchrotron and Large Hadron Collider to be explained and should be considered in design of the future accelerators.

DOI: [10.1103/PhysRevAccelBeams.27.074401](https://doi.org/10.1103/PhysRevAccelBeams.27.074401)

## I. INTRODUCTION

The interaction of charged particles with the accelerator environment (impedance) can result in the development of undamped or exponentially growing bunch oscillations in longitudinal [1] and transverse [2] planes. The broadband (BB) and narrowband (NB) impedances are responsible for single- and multibunch collective effects, respectively. In the absence of synchrotron radiation damping, beam stabilization is provided by the natural frequency spread of individual particles, called Landau damping [3], and accurate knowledge of the instability thresholds is necessary for a reliable accelerator design. Macroparticle simulations with realistic impedance models are still not feasible for thousands of bunches circulating in large-scale accelerators, such as the Large Hadron Collider (LHC), and cannot easily guide the parameter choice for the new accelerators (HL-LHC, EIC, FCC-hh, etc. [4–6]).

For the longitudinal beam motion considered below, a self-consistent set of equations determining beam stability for arbitrary impedance sources was derived in 1967 [7,8]. However, due to its complexity, a simplified method of the stability diagrams [9], developed initially for the coasting (unbunched) beams [10], is still commonly used (e.g., [11–14]). It was demonstrated [15] that the use of the stability diagrams [9] derived in a short-bunch approximation, significantly overestimates the threshold of coupled-bunch instability (CBI) driven by the high-frequency

NB impedance. In the low-frequency regime, the predictions are valid and were recently verified by an alternative approach and macroparticle simulations [16]. For the loss of Landau damping (LLD) caused by the BB (inductive or space-charge) impedance, thresholds similar to [9] were obtained in various studies [17–20], even if some discrepancy was found in numerical calculations [21] based on the Oide-Yokoya method [22].

As recently shown [23], the LLD threshold is in fact zero for the reactive impedance  $\text{Im}Z/k = \text{const}$  assumed in all previous studies unless a cutoff frequency  $f_c$  is introduced. Indeed, impedance  $\text{Im}Z_k/k$  decays at high frequencies  $f \gg c/b$  at least as  $k^{-3/2}$  [24,25], where  $k = f/f_0$  is a harmonic of the revolution frequency  $f_0$ , and  $b$  is a typical transverse size of the vacuum chamber. Some cutoff frequency is also naturally present in all numerical calculations and particle-tracking simulations. Then the LLD threshold is finite and it is inversely proportional to the impedance cutoff frequency  $f_c$  (defined, e.g., as  $Z = 0$  for  $f > f_c$ , see also discussion in Sec. III C). Therefore, the original stability diagrams give incorrect threshold values, except at a specific bunch length  $\tau \approx 1/f_c$ .

So far, the thresholds of CBI and LLD were calculated separately, with few examples when the CBI growth rates were found in the presence of two impedance sources [26,27]. In this work, for the first time, we develop a numerical approach to calculate self-consistently the instability threshold in the presence of both BB and NB impedances. A simple analytical expression for the generalized instability threshold is also proposed. The resulting multibunch instability has a mechanism different from CBI driven by the NB impedance only and can arise even below the LLD threshold. The results are confirmed by macroparticle simulations with a reduced number of bunches.

---

*Published by the American Physical Society under the terms of the Creative Commons Attribution 4.0 International license. Further distribution of this work must maintain attribution to the author(s) and the published article's title, journal citation, and DOI.*

This paper is organized in the following way. Section II introduces main equations and definitions required for the longitudinal beam stability analysis. A new approach to derive the instability threshold is described in Sec. III after a separate consideration of the CBI and LLD thresholds. Section IV discusses expectations for the HL-LHC and observations in CERN Super Proton Synchrotron (SPS). The work is summarized in Sec. V. Appendices A, B, and C contain detailed derivations of the induced voltage harmonics, the Oide-Yokoya matrix equation, and the instability growth rates, respectively.

## II. BEAM STABILITY ANALYSIS

Evaluation of beam stability is usually done in two steps. First, a stationary solution should be found, e.g., by the iterative procedure [21] for some particle distribution function, bunch intensity, and impedance model. To proceed with the second step, a small perturbation  $\tilde{\mathcal{F}} \propto e^{i\Omega t}$  to a stationary distribution function  $\mathcal{F}$  is considered, which should satisfy the linearized Vlasov equation. The beam is unstable if  $\text{Im}\Omega < 0$  for the coherent mode  $\Omega$ .

### A. A stationary case

Let us consider a beam of  $M$  identical and equidistant bunches, each containing  $N$  particles with a charge  $q$ . We use a coordinate system relative to the synchronous particle of the first bunch with the design energy  $E_0$  and the zero-intensity rf phase  $\phi_{s0}$ , so that  $\Delta E$  and  $\phi$  are the particle energy and rf phase deviations. The evolution of a single-particle position in conjugate coordinates  $\{\Delta E/(h\omega_0), \phi\}$  is governed by classical equations of motion (e.g., [28]):

$$\frac{d\phi}{dt} \equiv \dot{\phi} = \frac{h^2 \omega_0^2 \eta}{\beta^2 E_0} \left( \frac{\Delta E}{h\omega_0} \right), \quad (1)$$

$$\frac{d}{dt} \left( \frac{\Delta E}{h\omega_0} \right) = \frac{q}{2\pi h} [V_t(\phi) - V_t(0)]. \quad (2)$$

Here  $\omega_0$  is the angular revolution frequency,  $h$  the harmonic number,  $\eta = 1/\gamma_{\text{tr}}^2 - 1/\gamma^2$  the slip factor,  $\gamma$  the relativistic Lorentz factor with value  $\gamma_{\text{tr}}$  at transition energy, and  $\beta = \sqrt{1 - 1/\gamma^2}$ . The total voltage  $V_t(\phi) = V_{\text{rf}}(\phi) + V_{\text{ind}}(\phi)$  contains contributions from the rf field,  $V_{\text{rf}}(\phi)$ , and the stationary beam-induced voltage (see Appendix A):

$$V_{\text{ind}}(\phi) = -qMNh\omega_0 \sum_{k=-\infty}^{\infty} Z(k\omega_0) \lambda_k e^{ik\phi}, \quad (3)$$

with  $k = \omega/\omega_0$  and  $Z(\omega)$  being the longitudinal impedance. The Fourier harmonics of the line density

$$\lambda_k = \frac{1}{2\pi h} \int_{-\pi h}^{\pi h} \lambda(\phi) e^{-ik\phi} d\phi \quad (4)$$

are nonzero only for  $k = pM$ ,  $p = 0, \pm 1, \dots$ . The line density  $\lambda(\phi)$  is related to the stationary distribution function  $\mathcal{F}$  as

$$\lambda(\phi) = \int_{-\infty}^{\infty} \mathcal{F}(\phi, \dot{\phi}) d\dot{\phi},$$

and the normalization  $\int_{-\pi h}^{\pi h} \lambda(\phi) d\phi = 1$  is imposed.

For beam stability analysis, it is convenient to use another set of variables: the phase  $\psi$  and either action  $\mathcal{J}$  or energy  $\mathcal{E}$  of the synchrotron oscillations defined as

$$\mathcal{E} = \dot{\phi}^2 / (2\omega_{s0}^2) + U_t(\phi), \quad (5)$$

$$\psi = \text{sgn}(\eta \Delta E) \frac{\omega_s(\mathcal{E})}{\sqrt{2}\omega_{s0}} \int_{\phi_{\text{max}}}^{\phi} \frac{d\phi'}{\sqrt{\mathcal{E} - U_t(\phi')}}. \quad (6)$$

In this case, a stationary distribution function depends only on  $\mathcal{E}$  or  $\mathcal{J}$ , respectively, and not on  $\psi$ . Since  $\mathcal{J} \propto \int \dot{\phi}(\mathcal{E}) d\phi$ , the relation between  $\mathcal{J}$  and  $\mathcal{E}$  requires an additional integral to be numerically computed. Therefore, it is more efficient to use variables  $\{\mathcal{E}, \psi\}$  with the Jacobian of the transformation  $d\phi d\dot{\phi} = \omega_{s0}^2 d\psi d\mathcal{E}/\omega_s(\mathcal{E})$ .

Below, we consider only a single-rf case, when  $V_{\text{rf}}(\phi) = V_0 \sin(\phi_{s0} + \phi)$ , with  $V_0$  being the rf voltage amplitude. Then the angular frequency of small-amplitude synchrotron oscillations  $\omega_{s0}$  is

$$\omega_{s0} = \sqrt{-\frac{h\omega_0^2 \eta q V_0 \cos \phi_{s0}}{2\pi \beta^2 E_0}}. \quad (7)$$

The amplitude-dependent synchrotron frequency  $\omega_s(\mathcal{E}) = 2\pi/T_s(\mathcal{E})$  is defined by the period of oscillations

$$T_s(\mathcal{E}) = \frac{\sqrt{2}}{\omega_{s0}} \int_{\phi_{\text{min}}(\mathcal{E})}^{\phi_{\text{max}}(\mathcal{E})} \frac{d\phi'}{\sqrt{\mathcal{E} - U_t(\phi')}}}, \quad (8)$$

where the total potential

$$U_t(\phi) = \frac{1}{V_0 \cos \phi_{s0}} \int_{\Delta\phi_s}^{\phi} [V_t(\phi') - V_0 \sin \phi_{s0}] d\phi' \quad (9)$$

is modified by intensity effects (potential-well distortion). Here  $\phi_{\text{min}}(\mathcal{E})$  and  $\phi_{\text{max}}(\mathcal{E})$  are the minimum and maximum phases of the particle with the energy  $\mathcal{E}$  satisfying the condition  $\mathcal{E} = U_t(\phi_{\text{max}}) = U_t(\phi_{\text{min}})$ . The corresponding synchronous phase shift  $\Delta\phi_s$  is defined by the relation  $V_0 \sin \phi_{s0} = V_0 \sin(\phi_{s0} + \Delta\phi_s) + V_{\text{ind}}(\Delta\phi_s)$ .

### B. Time-dependent perturbation

Now, we consider a small, time-dependent perturbation  $\tilde{\mathcal{F}}$  to the stationary function  $\mathcal{F}(\mathcal{E})$ . For  $M$  equidistant bunches, the perturbation can be characterized by a coupled-bunch mode number  $l$  ( $l = 0, 1, \dots, M-1$ ),

corresponding to the rf phase advance  $2\pi l/M$  between consecutive bunches (see also Appendix A). Since the solution is a periodic function of  $\psi$ , it can be expanded in the Fourier series

$$\tilde{\mathcal{F}}^l(\mathcal{E}, \psi, t) = \tilde{\mathcal{F}}^l(\mathcal{E}, \psi, \Omega) e^{i\Omega t} = \sum_{m=-\infty}^{\infty} \tilde{\mathcal{F}}_m^l(\mathcal{E}, \Omega) e^{i\Omega t - im\psi} \quad (10)$$

with coefficients

$$\tilde{\mathcal{F}}_m^l(\mathcal{E}, \Omega) = \frac{1}{2\pi} \int_{-\pi}^{\pi} \tilde{\mathcal{F}}^l(\mathcal{E}, \psi, \Omega) e^{im\psi} d\psi, \quad (11)$$

where an azimuthal mode number  $m$  defines the type of interbunch oscillations (dipole, quadrupole, etc.).

The perturbation should satisfy the linearized Vlasov equation (see, e.g., [28]):

$$\left[ \frac{\partial}{\partial t} + \omega_s(\mathcal{E}) \frac{\partial}{\partial \psi} \right] \tilde{\mathcal{F}}^l = \omega_s(\mathcal{E}) \frac{\partial \tilde{U}_{\text{ind}}^l}{\partial \psi} \frac{d\mathcal{F}}{d\mathcal{E}}. \quad (12)$$

The corresponding perturbed induced potential  $\tilde{U}_{\text{ind}}^l$  is related to the perturbed induced voltage  $\tilde{V}_{\text{ind}}^l$ , derived in Appendix A:

$$\begin{aligned} \tilde{U}_{\text{ind}}^l(\phi, t) &= \frac{1}{V_0 \cos \phi_{s0}} \int_{\Delta\phi_s}^{\phi} \tilde{V}_{\text{ind}}^l(\phi', t) d\phi' \\ &= \frac{i\zeta M e^{i\Omega t}}{\cos \phi_{s0}} \sum_{k=-\infty}^{\infty} \frac{Z_k(\Omega)}{k} \tilde{\lambda}_k^l(\Omega) (e^{ik\phi/h} - e^{ik\Delta\phi_s/h}) \\ &= \tilde{U}_{\text{ind}}^l(\mathcal{E}, \psi, \Omega) e^{i\Omega t}, \end{aligned} \quad (13)$$

where the intensity parameter  $\zeta$  was defined as

$$\zeta = qN h^2 \omega_0 / V_0. \quad (14)$$

The Fourier harmonics of the perturbed line density are

$$\begin{aligned} \tilde{\lambda}_k^l(\Omega) &= \frac{1}{2\pi h} \int_{-\pi h}^{\pi h} \tilde{\lambda}^l(\phi, \Omega) e^{-ik\phi/h} d\phi \\ &= \frac{\omega_{s0}^2}{2\pi h} \int_{-\pi}^{\pi} d\psi \int_0^{\mathcal{E}_{\text{max}}} d\mathcal{E} \frac{\tilde{\mathcal{F}}^l(\mathcal{E}, \psi, \Omega)}{\omega_s(\mathcal{E})} e^{-ik\phi(\mathcal{E}, \psi)/h}. \end{aligned} \quad (15)$$

For any single-bunch intensity, there is an infinite number of solutions of Eq. (12), which can be described as van Kampen modes [21,29–31]. Most of them are defined by singular functions  $\tilde{\mathcal{F}}^l$  as they belong to the incoherent spectrum,  $\Omega \in m\omega_s(\mathcal{E})$ . Above a certain beam intensity, referred to as the threshold in this work, a coherent mode can emerge, which is then described by a regular function. For even higher intensity, more coherent modes can be present, each with specific dependency  $\tilde{\mathcal{F}}_m^l(\mathcal{E}, \Omega)$  on the radial variable  $\mathcal{E}$ . For a given  $m$ , the

number of oscillations of  $\tilde{\mathcal{F}}_m^l(\mathcal{E}, \Omega)$  within the bunch defines the radial-mode number  $n$ . The first self-consistent set of equations that allows finding coherent modes was proposed by Lebedev in 1967 [7,8]. Its derivation is briefly revisited below.

### C. Lebedev equation

The induced potential can be expanded as

$$\tilde{U}_{\text{ind}}^l(\phi, t) = e^{i\Omega t} \sum_{m=-\infty}^{\infty} \tilde{U}_{\text{ind},m}^l(\mathcal{E}, \Omega) e^{-im\psi}, \quad (16)$$

where based on Eq. (13),

$$\begin{aligned} \tilde{U}_{\text{ind},m}^l(\mathcal{E}, \Omega) &= \frac{1}{2\pi} \int_{-\pi}^{\pi} \tilde{U}_{\text{ind}}^l(\mathcal{E}, \psi, \Omega) e^{im\psi} d\psi \\ &= \frac{i\zeta}{\cos \phi_{s0}} \sum_{k=-\infty}^{\infty} \frac{Z_k(\Omega)}{k} \tilde{\lambda}_k^l(\Omega) I_{mk}(\mathcal{E}). \end{aligned} \quad (17)$$

Here the impedance  $Z_k(\Omega) = Z(k\omega_0 + \Omega)$ ,  $k = pM + l$ ,  $p = \pm 1, \pm 2, \dots$ . The function

$$I_{mk}(\mathcal{E}) = \frac{1}{2\pi} \int_{-\pi}^{\pi} e^{ik\phi(\mathcal{E}, \psi)/h + im\psi} d\psi \quad (18)$$

can be also written in a form that is convenient for the self-consistent numerical analysis [32]:

$$I_{mk}(\mathcal{E}) = \frac{ik}{h\pi m} \int_{\phi_{\text{min}}(\mathcal{E})}^{\phi_{\text{max}}(\mathcal{E})} e^{ik\phi/h} \sin[m\psi(\mathcal{E}, \phi)] d\phi. \quad (19)$$

Inserting Eqs. (10) and (16) into Eq. (12), one obtains

$$\begin{aligned} \tilde{\mathcal{F}}^l(\mathcal{E}, \psi, \Omega) &= \sum_{m=-\infty}^{\infty} \tilde{\mathcal{F}}_m^l(\mathcal{E}, \Omega) e^{-im\psi} \\ &= -\omega_s(\mathcal{E}) \frac{d\mathcal{F}}{d\mathcal{E}} \sum_{m=-\infty}^{\infty} \frac{m \tilde{U}_{\text{ind},m}^l(\mathcal{E}, \Omega)}{\Omega - m\omega_s(\mathcal{E})} e^{-im\psi}. \end{aligned} \quad (20)$$

Finally, combining Eqs. (15), (17), and (20), the Lebedev equation [7,8] reads as

$$\tilde{\lambda}_{k'}^l(\Omega) = \frac{\zeta M}{h \cos \phi_{s0}} \sum_{k=-\infty}^{\infty} G_{k'k}(\Omega) \frac{Z_k(\Omega)}{k} \tilde{\lambda}_k^l(\Omega). \quad (21)$$

The matrix elements  $G_{k'k}(\Omega)$  are

$$\begin{aligned}
G_{k'k} &= -\frac{i\omega_{s0}}{2\pi A} \sum_{m=-\infty}^{\infty} \int_0^{\mathcal{E}_{\max}} \frac{dg(\mathcal{E})}{d\mathcal{E}} \frac{I_{mk'}(\mathcal{E})I_{mk}^*(\mathcal{E})}{\Omega/m - \omega_s(\mathcal{E})} d\mathcal{E} \\
&= -\frac{\omega_{s0}}{2A} \operatorname{sgn}(\Omega) \sum_{m=1}^{\infty} \frac{dg(\mathcal{E}_m)/d\mathcal{E}}{d\omega_s(\mathcal{E}_m)/d\mathcal{E}} I_{mk'}(\mathcal{E}_m) I_{mk}^*(\mathcal{E}_m) \\
&\quad - i \frac{\omega_{s0}}{\pi A} \sum_{m=1}^{\infty} \mathcal{P} \int_0^{\mathcal{E}_{\max}} \frac{dg(\mathcal{E})}{d\mathcal{E}} \frac{I_{mk'}(\mathcal{E})I_{mk}^*(\mathcal{E})\omega_s(\mathcal{E})}{\Omega^2/m^2 - \omega_s^2(\mathcal{E})} d\mathcal{E},
\end{aligned} \tag{22}$$

where we introduced the function  $g(\mathcal{E}) = 2\pi\omega_{s0}A\mathcal{F}(\mathcal{E})$  with normalization

$$A = \omega_{s0} \int d\mathcal{E} g(\mathcal{E}) / \omega_s(\mathcal{E}).$$

The real part of the matrix element  $G_{k'k}$  appears if conditions  $\operatorname{Re}\Omega = m\omega_s(\mathcal{E}_m)$  and  $\operatorname{Im}\Omega \rightarrow 0^-$  are satisfied and is obtained by applying the rule

$$\lim_{\varepsilon \rightarrow 0^+} \frac{1}{x \pm i\varepsilon} = \mp i\pi\delta(x) + \mathcal{P}\left(\frac{1}{x}\right),$$

where  $\delta$  and  $\mathcal{P}$  denote the Dirac delta function and the principal value of the integral, respectively.

The coherent frequency  $\Omega = \Omega_g$  is the solution of general matrix equation (22) when the determinant

$$\det \left[ \delta_{k'k} - \frac{\zeta M}{h \cos \phi_{s0}} G_{k'k} \frac{Z_k}{k} \right] = \det(I - \zeta X) = 0, \tag{23}$$

where  $\delta_{k'k}$  is the Kronecker delta and  $I$  is the unity matrix. The beam is unstable if  $\operatorname{Im}\Omega_g < 0$ . The exact solution in a general case has to be obtained numerically, and we developed for this purpose the dedicated code MELODY [33]. Below, we also propose the approximate solution and discuss its validity.

### III. GENERALIZED INSTABILITY THRESHOLD

#### A. Approximate dispersion relation

As follows from Eq. (23), one of the eigenvalues of the matrix  $\zeta X$  equals one, e.g.,  $\nu_0 = 1$ . If  $\nu_n$  is the  $n$ th eigenvalue, so that

$$\det(\nu_n I - \zeta X) = 0,$$

then, based on the property of the matrix trace  $\operatorname{tr}(\zeta X) = \sum_n \nu_n$ , we have

$$\zeta = (1 + \sigma) / \operatorname{tr}(X), \tag{24}$$

where  $\sigma = \sum_{n \neq 0} \nu_n$  and

$$\operatorname{tr}(X) = \frac{M}{h \cos \phi_{s0}} \sum_{k=-\infty}^{\infty} \frac{Z_k(\Omega)}{k} G_{kk}(\Omega). \tag{25}$$

If one can estimate  $\sigma$  and show that it is small, the complexity of the problem is significantly reduced. Instead of computing all matrix elements, only the diagonal elements need to be evaluated.

Many impedance sources in the accelerator ring can be modeled by the resonances of the form:

$$Z(\omega) = \frac{R}{1 + iQ(\omega/\omega_r - \omega_r/\omega)}, \tag{26}$$

with a shunt impedance  $R$  and resonant frequency  $\omega_r$ . Typically, the quality factors  $Q \sim 1$  and  $Q \gg 1$  correspond to BB and NB impedances, respectively. We will show below that for these, most interesting, cases  $\sigma < 1$ , and the approximate threshold is

$$\zeta_{\text{th}} \approx 1 / \operatorname{tr}(X). \tag{27}$$

We will calculate the threshold  $\zeta$  by different numerical methods and estimate the value of  $\sigma$  for the various combinations of the NB and BB impedances.

#### B. Narrowband impedance: Coupled-bunch instability

Considering only the NB impedance, all elements in Eq. (21), except with  $k = k_{\text{nb}} = [\omega_{r,\text{nb}}/\omega_0]$ , can be neglected if

$$\Delta\omega_{\text{nb}} \ll M\omega_0, \quad \Delta\omega_{\text{nb}} \ll \left| \omega_{r,\text{nb}} - \frac{pM\omega_0}{2} \right|,$$

where  $\Delta\omega_{\text{nb}} = \omega_{r,\text{nb}}/2Q_{\text{nb}}$  is the resonator bandwidth, and  $[x]$  denotes the rounding of  $x$  to the nearest integer. In this case,  $\sigma = 0$  in Eq. (24), so that  $\nu_0 = 1$  is the only nonzero eigenvalue. Then, Eq. (27) is exact and can be rewritten in a form:

$$G_{k_{\text{nb}}k_{\text{nb}}}(\Omega) / \cos \phi_{s0} = \frac{k_{\text{nb}}h}{Z_{k_{\text{nb}}}(\Omega)\zeta M}. \tag{28}$$

The analytical expression for the NB threshold can be found by applying the method of threshold diagrams proposed in [15].

We consider a general class of distribution functions belonging to a binomial family

$$g(\mathcal{E}) = (1 - \mathcal{E}/\mathcal{E}_{\max})^\mu, \tag{29}$$

which covers a wide range of bunch shapes, from a water-bag ( $\mu = -1/2$ ) to Gaussian ( $\mu \rightarrow \infty$ ). First, we will derive the threshold for  $\mu \geq 1$  and then will briefly highlight the difference with the case of  $\mu < 1$  as well as with the distribution considered in the original work [15]:



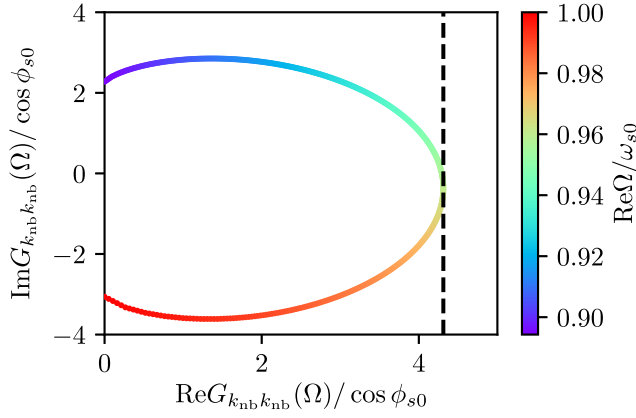


FIG. 1. Example of the threshold diagram given by  $G_{kk}$  from Eq. (22) and computed for  $\text{Re}\Omega \in [\omega_s(\mathcal{E}_{\max}), \omega_s(0)]$  with  $m \leq 3$  for  $k_{\text{nb}}/h = 11/9$ ,  $\mathcal{E}_{\max} = 0.73$  ( $\phi_{\max} = 1.3$ ),  $\mu = 2$  and  $\phi_{s0} = \pi$ . The vertical dashed line corresponds to maximum of  $\text{Re}G_{kk}/\cos\phi_{s0}$ .

$$g(\mathcal{E}) = \begin{cases} 1 - \frac{\mathcal{E}^2}{a\mathcal{E}_{\max}^2}, & 0 \leq \mathcal{E} < a\mathcal{E}_{\max} \\ \frac{1}{1-a} \left(1 - \frac{\mathcal{E}}{\mathcal{E}_{\max}}\right)^2, & a\mathcal{E}_{\max} \leq \mathcal{E} < \mathcal{E}_{\max}, \end{cases} \quad (30)$$

where  $0 < a < 1$ . Below, it will be referred to as a “flatten” distribution, since it can be obtained in operation after some beam manipulations (as, for example, rf phase modulation) reducing the peak line density. This technique was used in the past in the Tevatron to suppress oscillations of “dancing” bunches [34], and it is still applied during LHC physics to increase a full-width half-maximum bunch length [35].

The threshold diagram is a contour in the complex plane obtained from the left-hand side of Eq. (28) (colored curve in Fig. 1) by varying  $\Omega$ . The right-hand side of Eq. (28) corresponds to a vertical line, and its horizontal position is given by  $k_{\text{nb}}h/(R_{\text{nb}}\zeta M)$ . Crossing of the diagram and the vertical line for a certain mode frequency  $\Omega = \Omega_{\text{nb}}$  defines the threshold of instability. Therefore, the following conditions are satisfied simultaneously:

$$\text{Re}G_{k_{\text{nb}}k_{\text{nb}}}(\Omega_{\text{nb}})/\cos\phi_{s0} = \frac{k_{\text{nb}}h}{R_{\text{nb}}\zeta M}, \quad (31)$$

$$\text{Im}G_{k_{\text{nb}}k_{\text{nb}}}(\Omega_{\text{nb}})/\cos\phi_{s0} \approx \frac{k_{\text{nb}}h}{R_{\text{nb}}\zeta M} \frac{\omega_{\text{nb}} - \omega_{r,\text{nb}}}{\Delta\omega_{\text{nb}}}, \quad (32)$$

where  $\omega_{\text{nb}} = k_{\text{nb}}\omega_0 + \Omega_{\text{nb}}$ . If the resonator bandwidth  $\Delta\omega_{\text{nb}} \sim \omega_{s0}$ , the lowest instability threshold for distributions with  $\mu \geq 1$  corresponds to the maximum value of  $\text{Re}G_{k_{\text{nb}}k_{\text{nb}}}(\Omega_{\text{nb}})/\cos\phi_{s0}$  and defines  $\Omega_{\text{nb}}$  according to Eq. (31). In this case, the precise value of the resonance frequency  $\omega_{r,\text{nb}}$  is given by Eq. (32). Alternatively, if  $\Delta\omega_{\text{nb}} \gg \omega_{s0}$ , the right-hand side of Eq. (32) weakly depends on  $\Omega_{\text{nb}}$  and it is almost zero. Therefore, the threshold based on the maximum value of

$\text{Re}G_{k_{\text{nb}}k_{\text{nb}}}(\Omega_{\text{nb}})/\cos\phi_{s0}$  can slightly underestimate the actual threshold, as shown in Fig 1.

If we consider a stationary bucket (no acceleration) above transition energy ( $\phi_{s0} = \pi$ ) and neglect potential-well distortion, then, according to Eq. (22), Eq. (31) becomes

$$\frac{k_{\text{nb}}h}{R_{\text{nb}}\zeta M} = \frac{16\mu(\mu+1)}{\phi_{\max}^4} \text{sgn}(\Omega_{\text{nb}}) \times \sum_{m=1}^{\infty} \left(1 - \frac{\mathcal{E}_m}{\mathcal{E}_{\max}}\right)^{\mu-1} J_m^2\left(\frac{k_{\text{nb}}}{h} \sqrt{2\mathcal{E}_m}\right), \quad (33)$$

with  $\text{Re}\Omega_{\text{nb}} = m\omega_s(\mathcal{E}_m)$ .

This equation was obtained in a short-bunch approximation assuming that

$$\mathcal{E}_{\max} = 2\sin^2(\phi_{\max}/2) \approx \phi_{\max}^2/2,$$

$$\phi(\mathcal{E}, \psi) \approx \sqrt{2\mathcal{E}} \cos\psi,$$

$$\omega_s(\mathcal{E}) \approx \omega_{s0}(1 - \mathcal{E}/8).$$

In this case, from Eq. (18), we get  $I_{mk}(\mathcal{E}) \approx i^m J_m(k\sqrt{2\mathcal{E}}/h)$ , where  $\phi_{\max}$  is the half bunch length in the rf-phase radians, and  $J_m$  is the Bessel function of the first kind and the order  $m$ . The applicability range of this approximation can be estimated, for example, from the first line above: for  $\phi_{\max} \leq 1.3$  the relative error for  $\mathcal{E}_{\max}$  value is less than 15%.

The analysis of Eq. (33) shows that the NB instability threshold for  $\mu > 1$  and any  $k_{\text{nb}}$  is always the lowest for the dipole mode  $m = 1$ . Moreover, in our case, the contribution of higher-order azimuthal modes  $m$  is negligible, since the full synchrotron frequency spread, equal to  $\omega_{s0}\mathcal{E}_{\max}/8$ , is smaller than  $\omega_{s0}/2$ . Thus the threshold can be written as [36]

$$\zeta_{\text{th}}^{\text{nb}} = \frac{h\phi_{\max}^4 k_{\text{nb}}}{16\mu(\mu+1)MR_{\text{nb}}} \min_{x \in [0,1]} \left[ \frac{(1-x)^{1-\mu}}{J_1^2(k_{\text{nb}}\phi_{\max}\sqrt{x}/h)} \right]. \quad (34)$$

In the numerical calculations, we mainly use the LHC parameters at injection energy from Table I. An example of the stability analysis for the SPS parameters is shown in Sec. IV.

TABLE I. Accelerator and rf parameters of the LHC and Super Proton Synchrotron (SPS) at  $E_0 = 450$  GeV [4,37].

Parameter	Units	LHC	SPS
Circumference, $C$	m	26658.86	6911.55
Harmonic number, $h$		35640	4620
Transition gamma, $\gamma_{\text{tr}}$		55.76	17.95
rf frequency, $f_{\text{rf}}$	MHz	400.79	200.39
rf voltage, $V_0$	MV	6.0	7.0

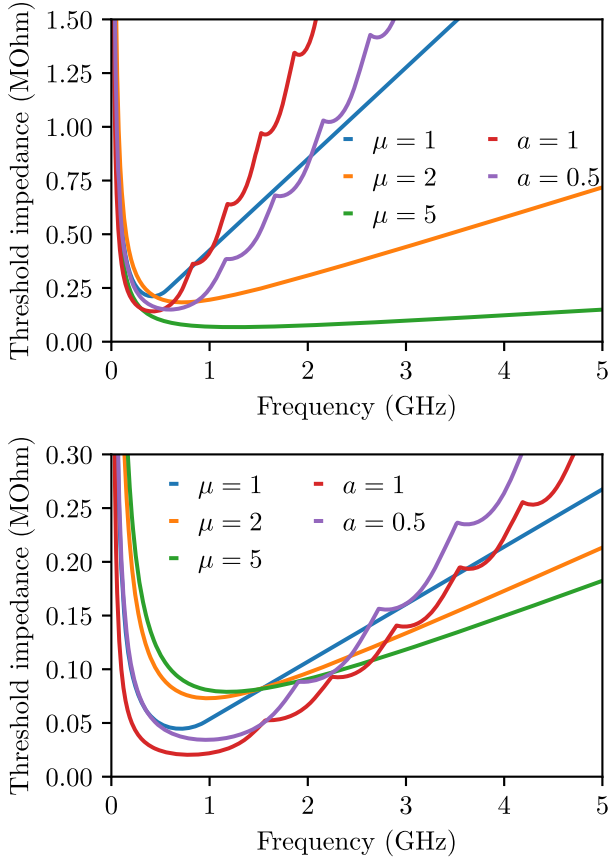


FIG. 2. Threshold shunt impedance for binomial (29) and flat (30) distribution functions in assumption of the same full bunch length with  $2\phi_{\max} = 2.6$  (top) and of the same effective bunch length,  $2\phi_{\text{eff}} = 1.6$  (bottom). The thresholds are calculated for the LHC parameters listed in Table I.

The threshold shunt impedance as a function of the resonant frequency found from Eq. (34) is shown in Fig. 2 for various distribution functions and two different bunch lengths (top and bottom figures). Keeping the same full bunch length,  $2\phi_{\max}$ , the threshold is typically higher for smaller  $\mu$  (top plot). However, in practice, the full bunch length is difficult to determine due to the noise in the measured signals. Therefore, it is common to use in operation [38,39], the effective bunch length obtained by scaling the half-width half-maximum (HWHM) bunch length with a factor  $\sqrt{2/\ln 2}$  (defined by a Gaussian distribution):

$$\phi_{\text{eff}} = \phi_{\text{HWHM}} \sqrt{2/\ln 2}. \quad (35)$$

In a short-bunch approximation, we have

$$\phi_{\text{HWHM}} = \phi_{\max} \sqrt{1 - 0.5^{\frac{2}{2\mu+1}}}.$$

For the same effective bunch length, the thresholds are very similar for  $\mu > 1$ , while the minimum threshold for  $\mu = 1$  is about 50% lower (see Fig. 2, bottom).

For binomial distribution with  $\mu < 1$ , the function  $dg/d\mathcal{E}$  diverges when  $\mathcal{E}_m \rightarrow \mathcal{E}_{\max}$ , and  $\text{Re}G_{k_{\text{nb}}k_{\text{nb}}} \rightarrow \infty$ . In this case,  $\text{Im}G_{k_{\text{nb}}k_{\text{nb}}}$  has to be evaluated numerically, and the threshold will be defined by a maximum value of  $\text{Re}G_{k_{\text{nb}}k_{\text{nb}}}$  for which  $\text{Im}G_{k_{\text{nb}}k_{\text{nb}}}(\Omega_{\text{nb}}) = 0$ .

Initially, the analytical threshold was found [15] for a specific type of distribution function (30) with zero derivative in the bunch center. Using another feature of this distribution, that its derivative has a minimum,  $-2/\mathcal{E}_{\max}$ , at  $\mathcal{E} = a\mathcal{E}_{\max}$ , one can obtain the threshold in the short-bunch approximation for  $a > 0.5$  [15]:

$$\zeta_{\text{th}}^{\text{nb}} = \frac{(1+a)h\phi_{\max}^4 k_{\text{nb}}}{96MR_{\text{nb}}} \min_{m \geq 1} \left[ J_m^{-2} \left( \frac{k_{\text{nb}}}{h} \phi_{\max} \sqrt{a} \right) \right]. \quad (36)$$

For  $a < 0.5$ , one has to search numerically for a minimum in both intervals  $\mathcal{E} \in [0, a\mathcal{E}_{\max}]$  and  $\mathcal{E} \in (a\mathcal{E}_{\max}, \mathcal{E}_{\max}]$ . Examples of the thresholds computed for this particle distribution function are shown in Fig. 2. The main difference in comparison with threshold (34) is that above a certain value of the resonance frequency, higher-order azimuthal mode ( $m > 1$ ) has the lowest CBI threshold (seen as a jump in its derivative). The distribution with  $a = 1$  has the lowest threshold in comparison to other distributions with the same effective half-bunch length, while above a certain resonant frequency, the binomial distribution functions give more conservative estimates.

The analytical predictions were compared with the self-consistent calculations done with the code MELODY based on two approaches: the Oide-Yokoya method [22] (see Appendix B) and direct evaluation of determinant (23). It allowed stability analysis for LHC parameters (Sec. IV) by treating each coupled-bunch mode separately in an assumption of the uniformly filled ring. Due to a very large number of the LHC bunches ( $\sim 3000$ ), particle-tracking simulations requiring many macroparticles are computationally too expensive. Although they exist for a few hundred bunches with up to  $10^5$  macroparticles per bunch (e.g., [40]), simulations for more than  $10^{10}$  of macroparticles (a few millions per bunch) remain a challenge even using modern techniques based on parallelization [41]. To overcome this limitation, some calculations were performed for nine equidistant bunches ( $M = 9$ ) by reducing the harmonic number to nine ( $h = 9$ ) and scaling other parameters to keep  $\zeta$  and  $\omega_{s0}/\omega_0$  unchanged. Once the numerical self-consistent calculations were confirmed with macroparticle simulations carried out with the particle-tracking code BLoND [42] (see Sec. III E), the predictions for unscaled parameters can be justified.

For a single NB resonator with  $k_{\text{nb}} = 11$ , a coupled-bunch mode  $l = 2$  should become unstable above a certain threshold, since  $k_{\text{nb}} = p \times M + l = 1 \times 9 + 2$ . Figure 3 (left) shows the dipole bunch-oscillation mode as a function of intensity. A mode with a coherent frequency inside the synchrotron frequency spread becomes unstable for

$\zeta > \zeta_{\text{th}}^{\text{nb}}$ , and the instability growth rate increases with intensity. The instability threshold found as the exact solution of Eq. (23) coincides with the emergence of the unstable mode. The solution (34) obtained in the short-bunch approximation gives about a 10% higher threshold for the bunch with  $\phi_{\text{max}} = 1.3$ .

### C. Broadband impedance: Loss of Landau damping

Assuming only a BB impedance, one can observe either LLD or single-bunch instability. Typically, the LLD threshold is lower, since the instability requires a significant potential-well distortion leading to the coupling of radial oscillation modes  $n$  with different or the same azimuthal mode numbers  $m$  [22,43,44]. Below, we revisit the recent evaluation of the LLD threshold [23] with a new analysis of its dependency on the cutoff frequency of BB impedance for different distribution functions.

For the case above transition energy (as in LHC) considered here, the dipole coherent mode typically emerges first above the maximum incoherent frequency  $\omega_s(0)$ , see Fig. 3 (center). Thus, at the LLD threshold  $\Omega = \Omega_{\text{bb}} = \omega_s(0)$ , the integral in Eq. (27) can be evaluated analytically for any  $k$ , and the contribution of higher-order azimuthal modes with  $m > 1$  can be neglected. It was also shown that the sum in Eq. (27) diverges linearly for impedance  $\text{Im}Z_k/k = \text{const}$  and distribution function (29), so some impedance cutoff frequency  $f_c$  should be introduced. The corresponding LLD threshold, derived in the short-bunch approximation, is

$$\zeta_{\text{th}}^{\text{bb}} = \frac{\pi\phi_{\text{max}}^5}{32\mu(\mu+1)\chi(k_{\text{eff}}\phi_{\text{max}}/h, \mu)} \frac{1}{(\text{Im}Z/k)_{\text{eff}}}. \quad (37)$$

The function

$$\chi(y, \mu) = y[1 - {}_2F_3(1/2, 1/2; 3/2, 2, \mu; -y^2)]$$

is approaching  $y$  for  $y \gg 1$ , and therefore,  $\zeta_{\text{th}}^{\text{bb}} \propto 1/k_{\text{eff}}$  for large  $k_{\text{eff}}$ . Above,  ${}_pF_q(a_1, \dots, a_p; b_1, \dots, b_q; z)$  is a generalized hypergeometric function and the effective impedance is defined as

$$(\text{Im}Z/k)_{\text{eff}} = \sum_{k=-k_{\text{eff}}}^{k_{\text{eff}}} G_{kk} \text{Im}Z_k/k \Big/ \sum_{k=-k_{\text{eff}}}^{k_{\text{eff}}} G_{kk}, \quad (38)$$

with the effective  $k_{\text{eff}}$ , which maximizes the cumulative sum in the nominator and plays the role of the cutoff frequency  $f_c = f_0 k_{\text{eff}}$ . Justification for the choice of  $f_c$  can be found in [45,46]. In practice, the effective cutoff can be estimated from beam-based measurements [47]. For a broadband resonator,  $k_{\text{eff}} = k_{\text{bb}} = \omega_{r,\text{bb}}/\omega_0$ . The elements  $G_{kk}$  can be expressed in terms of the generalized hypergeometric function:

$$G_{kk} = i \frac{16\mu(\mu+1)}{\pi\phi_{\text{max}}^4} \left[ 1 - {}_1F_2\left(\frac{1}{2}; 2, \mu; -y^2\right) \right], \quad (39)$$

where  $y = k\phi_{\text{max}}/h$ . For  $\mu = 2$ , one gets  $G_{kk} \propto [1/2 - J_0^2(y) - J_1^2(y) + J_0(y)J_1(y)/y]$  [23].

To verify the validity of the analytical threshold (37), we need to evaluate the relative contribution  $\sigma$  of eigenvalues of the matrix  $\zeta X$ . The matrix elements  $G_{k'k}$  can be approximated as

$$G_{k'k} \approx i \frac{16\mu(\mu+1)}{\pi\phi_{\text{max}}^4} \begin{cases} k'/k, & |k'| < |k| \\ k/k', & |k'| \geq |k|. \end{cases} \quad (40)$$

For this simple matrix and impedance  $\text{Im}Z_k/k = \text{const}$  truncated for  $|k| > f_c/f_0$ , the contribution of other eigenvalues is shown in Fig. 4. Since  $\sigma < 1$ , the maximum error in using Eq. (37) for the LLD threshold is a factor of 2. The eigenvectors of this matrix define the spectrum of the mode

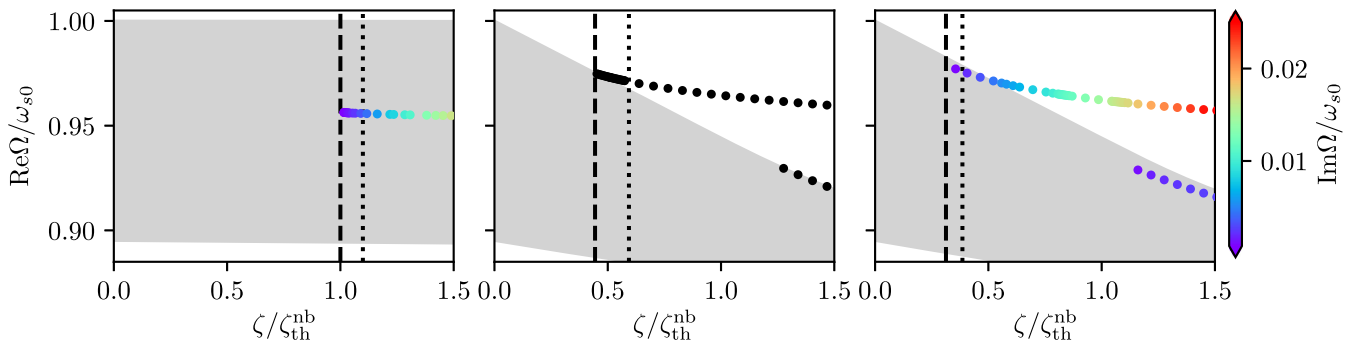


FIG. 3. Evolution of coherent dipole modes (black and colored circles) and incoherent frequency bands (gray) versus normalized intensity parameter  $\zeta$  defined in Eq. (14). Left: CBI with NB impedance. Center: LLD with BB impedance, no instability. Right: CBI with BB and NB impedances. Thresholds found with semianalytical code MELODY from Eq. (21) are shown with dashed lines while corresponding approximate solutions (37), (34), and (43) with dotted lines. The second dipole mode emerging at  $\zeta/\zeta_{\text{th}}^{\text{nb}} > 1$  is a higher-order radial mode. Examples for nine bunches in the scaled LHC ring with parameters from Table I and  $k_{\text{nb}}/h = 11/9$ ,  $Q_{\text{nb}} = 100$ ,  $R_{\text{nb}} = 37 \text{ k}\Omega$ ,  $k_{\text{bb}}/h = 5$ ,  $Q_{\text{bb}} = 1$ , and  $R_{\text{bb}} = 30 \text{ k}\Omega$ .

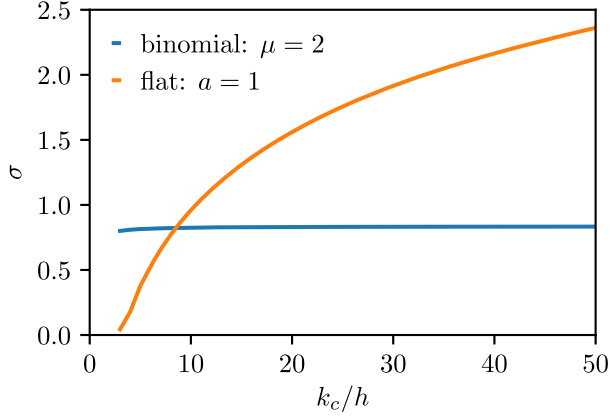


FIG. 4. Sum of eigenvalues (except  $\nu_0 = 1$ ) of the matrix  $\zeta X$  given by Eqs. (40) and (41) as functions of the cutoff frequency  $k_c f_0$  of inductive impedance  $\text{Im}Z_k/k = \text{const}$ . The value  $\zeta$  is chosen such that the maximum eigenvalue  $\nu_0 = 1$ . Other parameters:  $\phi_{\text{max}} = 1.3$  and  $h = 9$ .

at the LLD threshold. As was demonstrated in [23], the position of the maximum of the mode spectrum depends on the effective cutoff frequency of the impedance. For the truncated inductive impedance  $\text{Im}Z_k/k = \text{const}$ ,  $\max |\tilde{\lambda}_k^l(\Omega)|$  is located at  $\approx 0.63k_c$  (see Fig. 5). The higher the  $k_c$  is, the broader mode spectrum is, and it has a smaller amplitude at lower frequencies.

Similar analysis can be done for distribution function (30). For example, according to Eq. (27), the LLD threshold has a logarithmic dependency on the cutoff frequency, while the numerical solutions of Eq. (23) show that  $\zeta_{\text{th}}^{\text{bb}}$  does not depend on  $k_c$  [23]. For a distribution with  $a = 1$ , the  $G_{k'k}$  elements can be computed analytically in the short-bunch approximation:

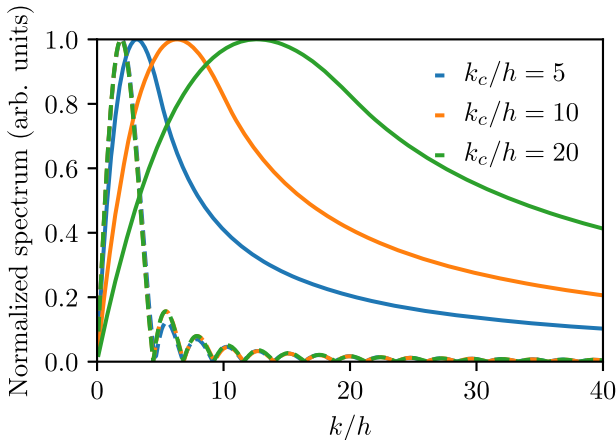


FIG. 5. Normalized spectra  $|\tilde{\lambda}_k^l(\Omega)|/\max |\tilde{\lambda}_k^l(\Omega)|$  of the largest eigenvalues ( $\nu_0 = 1$ ) of the matrix  $\zeta X$  given by Eqs. (40) (solid lines) and (41) (dashed lines) for different cutoff frequencies  $k_c f_0$  of inductive impedance  $\text{Im}Z_k/k = \text{const}$ . Main parameters:  $\mu = 2$ ,  $a = 1$ ,  $\phi_{\text{max}} = 1.3$ , and  $h = 9$ .

$$G_{k'k} = \frac{96i}{\pi\phi_{\text{max}}^4} \begin{cases} \frac{J_0^2(y_k)}{2} + \frac{J_1^2(y_k)}{2} - \frac{J_0(y)J_1(y_k)}{y_k}, & k = k' \\ \frac{y_{k'}J_0(y_{k'})J_1(y_k) - y_kJ_0(y_k)J_1(y_{k'})}{y_k^2 - y_{k'}^2}, & k \neq k' \end{cases}, \quad (41)$$

where  $y_k = k\phi_{\text{max}}/h$ . Evaluating numerically, we find that the maximum eigenvalue of the corresponding matrix  $\zeta X$  is not affected by increasing the cutoff frequency for  $k_c/h > \pi/\phi_{\text{max}}$ , and therefore, the LLD threshold does not depend on  $k_c$ . However,  $\sigma$  increases logarithmically as a function of  $k_c$  leading to the growth of the matrix trace as shown in Fig. 4. Thus, in this case, the LLD threshold can be evaluated according to Eq. (27) after the matrix truncation at  $k_c/h \approx \pi/\phi_{\text{max}}$ . Analyzing the eigenvalues at the LLD threshold, one can also see that the mode spectra do not depend on the cutoff frequency (dashed lines in Fig. 5).

The results of numerical calculations with MELODY for a pure BB resonator impedance are shown in Fig. 3 (center) together with the approximate threshold. The LLD mode emerges at  $\zeta = \zeta_{\text{th}}^{\text{bb}}$  above the maximum incoherent frequency  $\omega_s(0)$  leading to undamped but stable bunch oscillations. Similar to the case of NB impedance considered above, the LLD threshold computed from the Lebedev equation agrees with the Oide-Yokoya method. As one can see, the analytical approximation overestimates it by  $\sim 30\%$ , with  $|\sigma| < 0.3$  in the most cases [23].

## D. Broadband and narrowband impedances

Finally, if we combine the BB and NB impedances, the sum over  $k$  in Eq. (27) can be split into two terms, and the threshold  $\zeta_{\text{th}} = \zeta_{\text{th}}(\Omega_g)$  presented as

$$\begin{aligned} \frac{1}{\zeta_{\text{th}}} &\approx \frac{M}{h \cos \phi_{s0}} \sum_{k=-\infty}^{\infty} \frac{Z_k(\Omega_g)}{k} G_{kk}(\Omega_g) \\ &= \frac{M}{h \cos \phi_{s0}} \sum_{k \neq k_{\text{nb}}} \frac{\text{Im}Z_k(\Omega_g)}{k} G_{kk}(\Omega_g) \\ &\quad + \frac{M}{h \cos \phi_{s0}} \frac{\text{Re}Z_{k_{\text{nb}}}(\Omega_g)}{k_{\text{nb}}} G_{k_{\text{nb}}k_{\text{nb}}}(\Omega_g), \end{aligned} \quad (42)$$

where the contribution of the real part of  $Z_k$  in the sum is close to zero due to the symmetry  $G_{kk} = G_{-k-k}$ , while  $\text{Im}Z_{k_{\text{nb}}}$  can be neglected according to Eq. (32). The coherent mode  $\Omega_g$  for the general case differs from  $\Omega_{\text{nb}}$  and  $\Omega_{\text{bb}}$  found for each impedance separately. If  $\zeta_{\text{th}}^{\text{bb}}(\Omega_{\text{bb}}) \ll \zeta_{\text{th}}^{\text{nb}}(\Omega_{\text{nb}})$ ,  $\Omega_g \approx \Omega_{\text{bb}}$  and the NB instability threshold is reduced, as shown in Fig. 3 (right), where it is even below the LLD threshold. In the opposite case, the BB impedance has a negligible impact and  $\Omega_g \approx \Omega_{\text{nb}}$ . Although Eq. (42) should be solved numerically in the general case, we find that an approximate threshold

$$1/\zeta_{\text{th}} \approx 1/\zeta_{\text{th}}^{\text{nb}} + 1/\zeta_{\text{th}}^{\text{bb}} \quad (43)$$



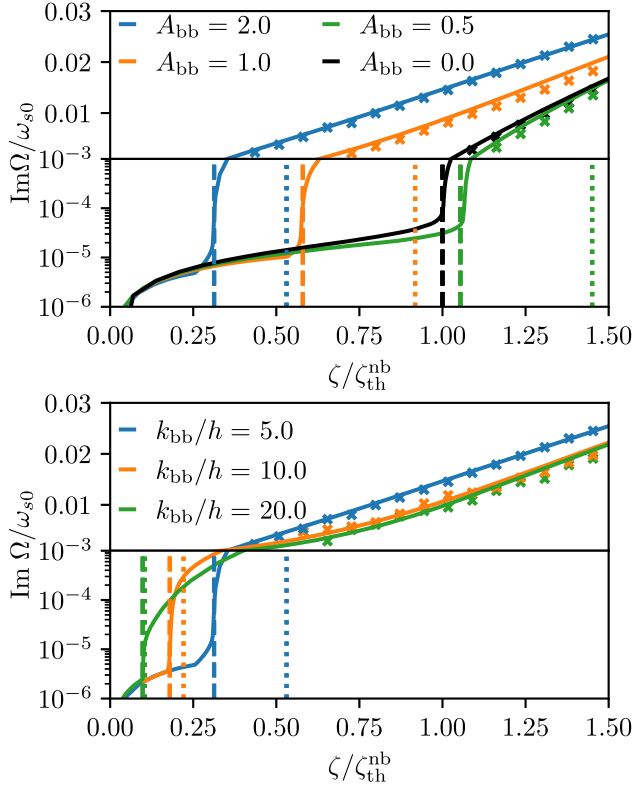


FIG. 6. Growth rate of the most unstable coupled-bunch mode ( $l = 2, m = 1$ ) versus the normalized intensity parameter  $\zeta$  for various strengths (top) and cutoff frequencies (bottom) of the BB impedance. Vertical lines show the LLD (dotted) and instability (dashed) thresholds found with MELODY from Eq. (21). The black dashed line corresponds to the NB impedance threshold. BLOND simulations are marked with crosses. The parameters from Table I were scaled to  $h = 9$ ;  $k_{nb}/h = 11/9$ ,  $Q_{nb} = 100$ ,  $R_{nb} = 37$  k $\Omega$ ,  $Q_{bb} = 1$ , and  $R_{bb} = 3A_{bb} \times (k_{bb}/h)$  k $\Omega$ . Top:  $k_{bb}/h = 5$  and bottom:  $A_{bb} = 2$ .

describes well the results of the full self-consistent calculations. For the binomial particle distribution (29),  $\zeta_{th}^{nb}$  and  $\zeta_{th}^{bb}$  are given by Eqs. (34) and (37), respectively. We also see from the numerical calculations that the resulting error for the general analytical expression (43) does not exceed the one for the LLD threshold.

The relative role of each contribution in Eq. (43) can be also seen in Fig. 6 from instability thresholds numerically obtained for different  $(\text{Im}Z/k)_{\text{eff}}$  and  $k_{bb}$  using Eq. (21). As expected, a larger BB impedance leads to a lower CBI threshold, except for the case when  $\zeta_{th}^{bb}(\Omega_{bb}) \gg \zeta_{th}^{nb}(\Omega_{nb})$ . The ratios of the CBI threshold with and without BB impedance  $\zeta_{th}/\zeta_{th}^{nb}$  support the analytical expression (43). For example, for  $A_{bb} = 2$ , one gets  $\zeta_{th}/\zeta_{th}^{nb} = 1/(1 + 1/0.53) \approx 0.35$  as compared to the value 0.31 found numerically from Eq. (21).

The impact of the parameter  $k_{\text{eff}}$  (related to the cutoff frequency) on the CBI is shown in Fig 6 (bottom). The CBI threshold is reduced for larger  $k_{bb}$ , since the LLD threshold

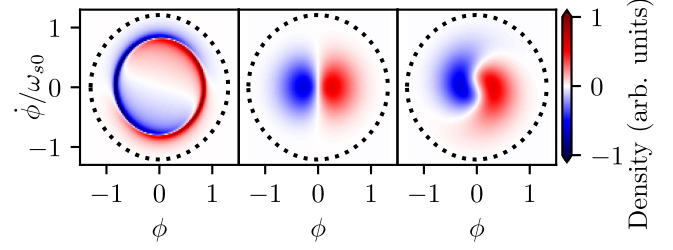


FIG. 7. Perturbed particle distribution function  $\tilde{\mathcal{F}}(\phi, \phi)$  in phase space for the unstable mode driven by NB impedance at  $\zeta/\zeta_{th}^{nb} = 1.1$  (left), LLD mode due to BB impedance only at  $\zeta/\zeta_{th}^{nb} = 0.5$  (center), and for the unstable mode with NB and BB impedance sources together at  $\zeta/\zeta_{th}^{nb} = 0.5$  (right). The dotted line is the outermost particle trajectory in the bunch. Other parameters are as in Fig. 3.

is lower and its overall effect in Eq. (43) is bigger. We see, however, that the growth rates above a certain intensity become smaller for larger  $k_{bb}$ . For larger  $k_{bb}$ , the mode spectrum shifts toward higher frequencies as for LLD mode [23] (solid lines in Fig. 5) and for  $k_{nb} < k_{bb}$  interacts weaker with NB impedance, according to Eq. (C2). This effect can be also illustrated by the character of perturbation in longitudinal phase space. For NB impedance ( $Z_{bb} = 0$ ), it mainly involves high-amplitude particles (see Fig 7, left), while the perturbation looks very different for the case of a single-bunch LLD and it is located in the bunch center (Fig 7, center). For this new mechanism of coupled-bunch instability in the presence of BB impedance, the mode is also localized in the bunch center (Fig 7, right).

### E. Comparison with macroparticle simulations

For comparison of the results obtained with the code MELODY and analytical approximations with macroparticle simulations, we deployed the code BLOND [42]. In the present work, up to  $4 \times 10^6$  macroparticles per bunch were tracked for a few hundred synchrotron periods. The expected coupled-bunch mode was seeded at the start of simulations by applying an initial kick with an amplitude of 0.1 deg to the rf phase of each bunch. The mean values of particle coordinates for each bunch were computed turn-by-turn, and the fit was performed to extract the growth rate of instability. The results of macroparticle simulations follow closely the growth rates obtained using the Oide-Yokoya method, as can be seen in Fig. 6.

## IV. EXAMPLES FOR LHC AND SPS

The effect of a low LLD threshold on the CBI threshold can be seen for the LHC beam in the full ring with parameters without scaling (Table I). In this case, the lowest CBI threshold due to a higher-order mode (HOM) of the future crab cavities [4] with  $R_{nb} = 280$  k $\Omega$ ,  $f_{r,nb} = 582$  MHz, and  $Q_{nb} = 1360$  calculated with

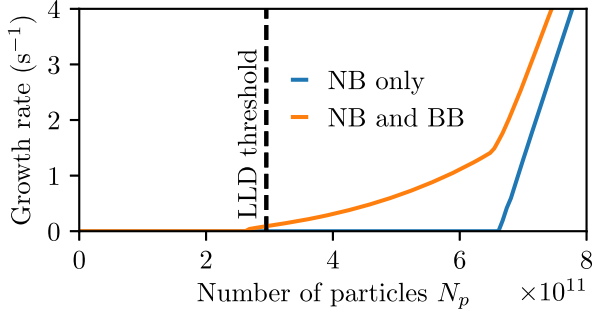


FIG. 8. Growth rates of multibunch instability versus bunch intensity calculated for LHC with  $M = h/10$ ,  $\phi_{\max} = 2.4$  (see Table I) and NB impedance with  $R_{\text{nb}} = 280$  k $\Omega$ ,  $f_{r,\text{nb}} = 582$  MHz, and  $Q_{\text{nb}} = 1360$ , in two cases: with (orange) and without (blue) BB impedance having  $R_{\text{bb}} = 38$  k $\Omega$ ,  $f_{r,\text{bb}} = 5$  GHz, and  $Q_{\text{bb}} = 1$ .

MELODY in the presence of BB impedance is 3 times smaller (see Fig. 8) [48].

The Super Proton Synchrotron (SPS) at CERN, being the LHC injector, also provides beams for the fixed-target experiments. These beams, filling the whole SPS ring, are different from the LHC-type trains. The CBI is driven by an HOM of the main 200 MHz rf system with  $f_r \approx 915$  MHz [49]. The CBI thresholds, found for the realistic SPS impedance model [50,51] and for the HOM impedance only, practically coincide (see Fig. 9), since in this case, the CBI threshold is lower than the LLD threshold by an order of magnitude due to a low single-bunch intensity. If the bunches fill every fifth rf bucket (as LHC-type beams), the HOM-driven CBI threshold is higher and the resulting threshold is more affected by the BB part of the SPS impedance. This explains why the LHC bunch train in the SPS has a very low CBI threshold, which also weakly depends on the number of bunches in a train [48]. To deliver high-intensity LHC beams, an additional 800-MHz

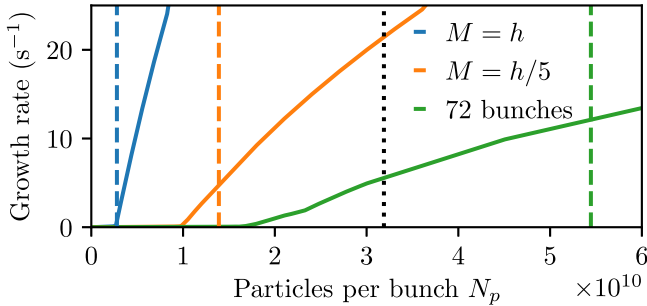


FIG. 9. Growth rates of the most unstable coupled-bunch mode (solid lines) versus bunch intensity for the SPS with  $M = h$  (blue),  $M = h/5$  (orange), and LHC-type train of 72 bunches spaced by  $5/f_{\text{rf}}$  (green). The corresponding CBI thresholds driven by an HOM at 915 MHz only (dashed lines). The LLD threshold is shown by a black dotted line. The SPS parameters from Table I, zero-intensity  $\phi_{\max} = 0.9$ , and  $\mu = 1.5$ . Calculations with code MELODY.

rf system, increasing the synchrotron frequency spread and the CBI threshold, is routinely deployed in operation [37].

## V. CONCLUSIONS

We proposed the approach to analyze beam stability in the presence of both broadband and narrowband impedance sources. The broadband impedance can significantly reduce the threshold of coupled-bunch instability driven by the narrowband impedance, and there is a new instability mechanism associated with it. The proposed generalized analytical expression shows the key role of the LLD threshold and demonstrates how two impedance contributions add up. For the LLD-dominated case, the values of the effective BB impedance and its cutoff frequency play an important role. The main conclusions are verified by macroparticle simulations and they are consistent with beam observations in the SPS. This understanding can help in finding mitigation measures aimed at increasing Landau damping for the existing high-current synchrotrons and should also be taken into account in design of the future rings.

## ACKNOWLEDGMENTS

We are grateful to Heiko Damerau for his useful comments.

## APPENDIX A: MULTIBUNCH INDUCED VOLTAGE

For  $M$  equidistant bunches in the ring, the perturbation of the distribution function of  $j$ th bunch can be written as follows:

$$\tilde{\mathcal{F}}_j^l(\mathcal{E}, \psi, t) = \tilde{\mathcal{F}}^l(\mathcal{E}, \psi, \Omega) e^{i\Omega(t-jT_0/M)} e^{-i2\pi l j/M},$$

where  $l = 0, 1, \dots, M-1$  is the coupled-bunch mode number. The corresponding line density is

$$\begin{aligned} \tilde{\lambda}_j^l(\phi, \Omega, t) &= \int_{-\infty}^{\infty} \tilde{\mathcal{F}}_j^l(\mathcal{E}, \psi, t) d\phi \\ &= 2\omega_{s0} \int_{U_t(\phi)}^{\mathcal{E}_{\max}} \frac{\tilde{\mathcal{F}}_j^l(\mathcal{E}, \psi, t)}{\sqrt{\mathcal{E} - U_t(\phi)}} d\mathcal{E} \\ &= \tilde{\lambda}^l(\phi, \Omega) e^{i\Omega(t-jT_0/M)} e^{-i2\pi l j/M}, \end{aligned} \quad (\text{A1})$$

with

$$\tilde{\lambda}^l(\phi, \Omega) = 2\omega_{s0} \int_{U_t(\phi)}^{\mathcal{E}_{\max}} \frac{\tilde{\mathcal{F}}^l(\mathcal{E}, \psi, \Omega)}{\sqrt{\mathcal{E} - U_t(\phi)}} d\mathcal{E}. \quad (\text{A2})$$

Since in the stationary case all bunches are indistinguishable, there is a free choice of the zeroth bunch. Its induced voltage, including contributions from other bunches and previous turns, can be written in the form

$$\begin{aligned} \tilde{V}_{\text{ind},0}^l(\phi, t) &= -qN \int_{-\infty}^{\infty} d\phi' \sum_{k=0}^{\infty} \tilde{\lambda}^l(\phi', \Omega) \\ &\times \sum_{j=0}^{M-1} W\left(\phi - \phi' + 2\pi hk + \frac{2\pi hj}{M}\right) \\ &\times e^{i\Omega(t-kT_0-jT_0/M)} e^{-i2\pi lj/M}. \end{aligned} \quad (\text{A3})$$

Here,  $W$  is the wake function, and the sum can be also extended to  $k < 0$  because of causality [ $W(\phi < 0) = 0$ ]. Below we will omit index 0 in the derivations. Using the connection of the wake function with impedance

$$W(\phi) = \frac{1}{2\pi} \int_{-\infty}^{\infty} Z(\omega) e^{i\omega\phi/\omega_{\text{rf}}} d\omega, \quad (\text{A4})$$

one obtains

$$\begin{aligned} \tilde{V}_{\text{ind}}(\phi, t) &= -\frac{qN}{2\pi} e^{i\Omega t} \int_{-\infty}^{\infty} \tilde{\lambda}^l(\phi', \Omega) d\phi' \\ &\times \int_{-\infty}^{\infty} Z(\omega) e^{i\omega(\phi-\phi')/\omega_{\text{rf}}} d\omega \\ &\times \sum_{k=-\infty}^{\infty} e^{i2\pi k(\omega-\Omega)/\omega_0} \sum_{j=0}^{M-1} e^{ijT_0(\omega-l\omega_0-\Omega)/M}. \end{aligned} \quad (\text{A5})$$

Here the first sum is the Dirac comb and the second sum

$$\sum_{j=0}^{M-1} e^{ijT_0(\omega-l\omega_0-\Omega)/M} = \frac{1 - e^{iT_0(\omega-l\omega_0-\Omega)}}{1 - e^{iT_0(\omega-l\omega_0-\Omega)/M}}.$$

Using these relations and performing integration over  $\omega$ , the induced voltage can be written as

$$\begin{aligned} \tilde{V}_{\text{ind}}(\phi, t) &= -qNh\omega_0 e^{i\Omega t} \\ &\times \sum_{k=-\infty}^{\infty} Z_k(\Omega) \tilde{\lambda}_k^l(\Omega) e^{ik\phi/h} e^{i\Omega\phi/\omega_{\text{rf}}} \\ &\times \frac{1 - e^{i2\pi(k-l)}}{1 - e^{i2\pi(k-l)/M}}, \end{aligned} \quad (\text{A6})$$

where  $Z_k = Z(k\omega_0 + \Omega)$ . The last term in Eq. (A6) is nonzero only for  $k = pM + l$ , where  $p = 0, \pm 1, \pm 2, \dots$ . Applying L'Hopital's rule,

$$\frac{1 - e^{i2\pi pM}}{1 - e^{i2\pi p}} = \lim_{x \rightarrow 2\pi} \frac{1 - e^{ixpM}}{1 - e^{ixp}} = \lim_{x \rightarrow 2\pi} \frac{-ipMe^{ixpM}}{-ipe^{ixp}} = M,$$

and finally we get the induced voltage in the multibunch case:

$$\begin{aligned} \tilde{V}_{\text{ind}}^l(\phi, t) &= -qMNh\omega_0 e^{i\Omega t} \\ &\times \sum_{k=-\infty}^{\infty} Z_k(\Omega) \tilde{\lambda}_k^l(\Omega) e^{ik\phi/h} e^{i\Omega\phi/\omega_{\text{rf}}}, \end{aligned} \quad (\text{A7})$$

with the harmonic of the line-density perturbation

$$\tilde{\lambda}_k^l(\Omega) = \frac{1}{2\pi h} \int_{-\pi h}^{\pi h} d\phi \tilde{\lambda}^l(\phi, \Omega) e^{-ik\phi/h} e^{-i\Omega\phi/\omega_{\text{rf}}}, \quad (\text{A8})$$

where  $k = pM + l$ . Typically, the phase factor  $e^{\pm i\Omega\phi/\omega_{\text{rf}}}$  in the equations above can be neglected since  $\Omega \approx m\omega_{s0} \ll \omega_0$  for low azimuthal modes  $m = 1, 2, 3, \dots$

To obtain the induced voltage in the stationary situation, it is sufficient to set in Eqs. (A7) and (A8)  $\Omega \rightarrow 0$  and  $l \rightarrow 0$  leading to

$$V_{\text{ind}}(\phi) = -qMNh\omega_0 \sum_{k=-\infty}^{\infty} Z(k\omega_0) \lambda_k e^{ik\phi/h}, \quad (\text{A9})$$

with

$$\lambda_k = \frac{1}{2\pi h} \int_{-\pi h}^{\pi h} \lambda(\phi, \Omega) e^{-ik\phi/h} d\phi \quad (\text{A10})$$

and, naturally,  $k = pM$ .

## APPENDIX B: OIDE-YOKOYA METHOD

The Oide-Yokoya method was developed for the numerical study of longitudinal single-bunch instabilities [22]. Here, we consider its application to the multibunch stability case.

The perturbed distribution function  $\tilde{\mathcal{F}}^l(\mathcal{E}, \psi, \Omega)$  in Eq. (10) can be presented in the form

$$\tilde{\mathcal{F}}^l(\mathcal{E}, \psi, \Omega) = \sum_{m=1}^{\infty} C_m^l(\mathcal{E}, \Omega) \left[ \cos m\psi - \frac{i\Omega}{m\omega_s(\mathcal{E})} \sin m\psi \right], \quad (\text{B1})$$

where  $C_m^l(\mathcal{E}, \Omega)$  are the functions describing the type of perturbation. Inserting  $\tilde{\mathcal{F}}^l(\mathcal{E}, \psi, t)$  in Vlasov equation (12), multiplying it by  $\sin m\psi$ , and integrating by  $\psi \in (-\pi, \pi)$ , one obtains the following equation:

$$\begin{aligned} C_m^l(\mathcal{E}, \Omega) \pi \left[ \frac{\Omega^2}{m\omega_s} - m\omega_s \right] \\ = -m\omega_s(\mathcal{E}) \frac{d\mathcal{F}}{d\mathcal{E}} \int_{-\pi}^{\pi} d\psi \tilde{U}_{\text{ind}}(\mathcal{E}, \psi, \Omega) \cos m\psi \\ = -\frac{i2\pi M\zeta m\omega_s(\mathcal{E}) d\mathcal{F}}{h \cos \phi_{s0}} \sum_{k=-\infty}^{\infty} \frac{Z_k(\Omega)}{k} \tilde{\lambda}_k^l(\Omega) I_{mk}(\mathcal{E}). \end{aligned} \quad (\text{B2})$$

Note that here  $k = pM + l$  with  $p = 0, \pm 1, \pm 2, \dots$ , which is the main difference from the single-bunch case, where all

harmonics are present in the sum. To obtain the final integral equation, the perturbed harmonics of the line density need to be expressed via  $C_m^l(\mathcal{E}, \Omega)$ . Thus, substituting  $\tilde{\mathcal{F}}^l$  into Eq. (15) by functions (B1), we get

$$\tilde{\lambda}_k^l(\Omega) = \frac{\omega_{s0}^2}{h} \sum_{m=1}^{\infty} \int_0^{\mathcal{E}_{\max}} d\mathcal{E} \frac{C_m^l(\mathcal{E}, \Omega) I_{mk}^*(\mathcal{E})}{\omega_s(\mathcal{E})}, \quad (\text{B3})$$

and their further insertion into Eq. (B2) leads to

$$\begin{aligned} & \left[ \frac{\Omega^2}{\omega_{s0}^2} - \frac{m^2 \omega_s^2(\mathcal{E})}{\omega_{s0}^2} \right] C_m^l(\mathcal{E}, \Omega) \\ &= - \frac{2iM\zeta m^2 \omega_s^2(\mathcal{E})}{h \cos \phi_{s0}} \frac{d\mathcal{F}(\mathcal{E})}{d\mathcal{E}} \sum_{m'=1}^{\infty} \int_0^{\mathcal{E}_{\max}} \frac{d\mathcal{E}'}{\omega_s(\mathcal{E}')} \\ & \times \sum_{k=-\infty}^{\infty} \frac{Z_k(\Omega)}{k} I_{mk}(\mathcal{E}) I_{m'k}^*(\mathcal{E}') C_{m'}^l(\mathcal{E}', \Omega). \end{aligned} \quad (\text{B4})$$

In the original work [22], the functions equivalent to  $C_m^l(\mathcal{E}, \Omega)$  were defined as a combination of the step-like functions. It is convenient, however, for further analysis of the instability growth rates to perform a substitution:

$$C_m^l(\mathcal{E}, \Omega) = \sqrt{-\omega_s(\mathcal{E}) \frac{d\mathcal{F}(\mathcal{E})}{d\mathcal{E}}} m \frac{\omega_s(\mathcal{E})}{\omega_{s0}^2} \tilde{C}_m^l(\mathcal{E}, \Omega) \quad (\text{B5})$$

and introduce a set of orthonormal functions  $s_n^{(m)}$

$$\int_0^{\mathcal{E}_{\max}} s_n^{(m)}(\mathcal{E}) s_{n'}^{(m)}(\mathcal{E}) d\mathcal{E} = \delta_{nn'}.$$

Then, Eq. (B4) becomes

$$\begin{aligned} & \left[ \frac{\Omega^2}{\omega_{s0}^2} - \frac{m^2 \omega_s^2(\mathcal{E})}{\omega_{s0}^2} \right] \tilde{C}_m^l(\mathcal{E}, \Omega) \\ &= -2i\zeta \sum_{m'=1}^{\infty} \int_0^{\mathcal{E}_{\max}} K_{mm'}(\mathcal{E}, \mathcal{E}') \tilde{C}_{m'}^l(\mathcal{E}', \Omega) d\mathcal{E}', \end{aligned} \quad (\text{B6})$$

where the kernel  $K_{mm'}$  is defined as

$$\begin{aligned} K_{mm'}(\mathcal{E}, \mathcal{E}', \Omega) &= \sum_{k=-\infty}^{\infty} \frac{Z_k(\Omega)/k}{hZ_0} \\ & \times m \sqrt{-\omega_s(\mathcal{E}) \frac{d\mathcal{F}(\mathcal{E})}{d\mathcal{E}}} I_{mk}(\mathcal{E}) \\ & \times m' \sqrt{-\omega_s(\mathcal{E}') \frac{d\mathcal{F}(\mathcal{E}')}{d\mathcal{E}'}} I_{m'k}^*(\mathcal{E}'). \end{aligned} \quad (\text{B7})$$

The next step is to decompose  $\tilde{C}_m^l$  and  $K_{mm'}$ , similar to [31]:

$$\tilde{C}_m^l(\mathcal{E}, \Omega) = \sum_{n=0}^{\infty} \tilde{C}_m^{ln}(\Omega) s_n^{(m)}(\mathcal{E}), \quad (\text{B8})$$

$$K_{mm'}(\mathcal{E}, \mathcal{E}', \Omega) = \sum_{n=0}^{\infty} \sum_{n'=0}^{\infty} K_{mm'}^{nn'}(\Omega) s_n^{(m)}(\mathcal{E}) s_{n'}^{(m')}(\mathcal{E}'), \quad (\text{B9})$$

with the coefficients

$$\tilde{C}_m^{ln}(\Omega) = \int_0^{\mathcal{E}_{\max}} \tilde{C}_m^l(\mathcal{E}, \Omega) s_n^{(m)}(\mathcal{E}) d\mathcal{E}, \quad (\text{B10})$$

and

$$K_{mm'}^{nn'}(\Omega) = \int_0^{\mathcal{E}_{\max}} \int_0^{\mathcal{E}_{\max}} K_{mm'}(\mathcal{E}, \mathcal{E}', \Omega) s_n^{(m)}(\mathcal{E}) s_{n'}^{(m')}(\mathcal{E}') d\mathcal{E} d\mathcal{E}'. \quad (\text{B11})$$

Finally, one obtains the following system of equations:

$$\frac{\Omega^2}{\omega_{s0}^2} \tilde{C}_m^{ln}(\Omega) = \sum_{n'=0}^{\infty} \sum_{m'=1}^{\infty} M_{mm'}^{nn'}(\Omega) \tilde{C}_{m'}^{ln'}(\Omega), \quad (\text{B12})$$

where the matrix elements are defined as

$$\begin{aligned} M_{mm'}^{nn'}(\Omega) &= m^2 \delta_{mm'} \int_0^{\mathcal{E}_{\max}} \frac{\omega_s^2(\mathcal{E})}{\omega_{s0}^2} s_n^{(m)}(\mathcal{E}) s_{n'}^{(m)}(\mathcal{E}) d\mathcal{E} \\ & - 2i\zeta K_{mm'}^{nn'}(\Omega). \end{aligned} \quad (\text{B13})$$

Choosing the step-like orthogonal functions

$$s_n^{(m)}(\mathcal{E}) = \begin{cases} \frac{1}{\sqrt{\Delta\mathcal{E}_n}}, & \mathcal{E}_n - \frac{\Delta\mathcal{E}_n}{2} < \mathcal{E} \leq \mathcal{E}_n + \frac{\Delta\mathcal{E}_n}{2} \\ 0, & \text{elsewhere,} \end{cases}$$

the matrix, equivalent to the one introduced in [22], is

$$\begin{aligned} M_{mm'}^{nn'}(\Omega) &= \frac{m^2 \omega_s^2(\mathcal{E}_n)}{\omega_{s0}^2} \delta_{nn'} \delta_{mm'} \\ & - 2i\zeta \sqrt{\Delta\mathcal{E}_n \Delta\mathcal{E}_{n'}} K_{mm'}(\mathcal{E}_n, \mathcal{E}_{n'}, \Omega). \end{aligned} \quad (\text{B14})$$

Since the number of orthogonal functions is finite, the system of Eq. (B12) becomes finite. Additionally, the sum over harmonics  $k$  has to be also truncated and the dependency of the impedance  $Z_k(k\omega_0 + \Omega)$  on  $\Omega$  has to be neglected. Therefore, the eigenvalues  $\Omega^2/\omega_{s0}^2$  and eigenvectors  $\tilde{C}_m^{ln}$  can be found by solving a standard eigenvalue problem.

### APPENDIX C: INSTABILITY GROWTH RATES

To derive the instability grow rates, we multiply Eq. (B6) by  $\tilde{C}_m^{l*}(\mathcal{E}, \Omega)$  and integrate over  $\mathcal{E}$ :



$$\begin{aligned} \Omega^2 = & \sum_{m=1}^{\infty} \int_0^{\mathcal{E}_{\max}} m^2 \omega_s^2(\mathcal{E}) \frac{|\tilde{C}_m^l(\mathcal{E}, \Omega)|^2}{B^l(\Omega)} d\mathcal{E} \\ & + \frac{2\zeta h \omega_{s0}^2}{B^l(\Omega)} \sum_{k=-\infty}^{\infty} \frac{\text{Im}Z_k(\Omega)}{k} |\tilde{\lambda}_k^l(\Omega)|^2 \\ & - \frac{2i\zeta h \omega_{s0}^2}{B^l(\Omega)} \sum_{k=-\infty}^{\infty} \frac{\text{Re}Z_k(\Omega)}{k} |\tilde{\lambda}_k^l(\Omega)|^2, \quad (\text{C1}) \end{aligned}$$

where

$$B^l(\Omega) = \sum_{m=1}^{\infty} \int_0^{\mathcal{E}_{\max}} |\tilde{C}_m^l(\mathcal{E}, \Omega)|^2 d\mathcal{E}.$$

In the case of instability, the eigenfunctions become regular functions, and we obtain

$$\text{Im}\Omega = -\frac{\zeta h \omega_{s0}^2}{B^l(\Omega) \text{Re}\Omega} \sum_{k=-\infty}^{\infty} \frac{\text{Re}Z_k(\Omega)}{k} |\tilde{\lambda}_k^l(\Omega)|^2. \quad (\text{C2})$$

For a combination of narrowband and broadband impedances (see Sec. III D), the growth rate is dominated by the spectral harmonic  $\tilde{\lambda}_k$  at  $k = k_{\text{nb}}$  for the narrowband resonant frequency  $k_{\text{nb}} f_0$ .

- 
- [1] C. E. Nielsen, A. M. Sessler, and K. R. Symon, Longitudinal instabilities in intense relativistic beams, in *Proceedings of the 2nd International Conference on High-Energy Accelerators, HEACC-1959, Geneva, Switzerland* (CERN, Geneva, Switzerland, 1959), pp. 239–252.
- [2] L. J. Laslett, V. K. Neil, and A. M. Sessler, Transverse resistive instabilities of intense coasting beams in particle accelerators, *Rev. Sci. Instrum.* **36**, 436 (1965).
- [3] L. D. Landau, On the vibrations of the electronic plasma, *J. Phys. (Moscow)* **10**, 25 (1946).
- [4] High-Luminosity Large Hadron Collider (HL-LHC): CERN Yellow Reports: Monographs, Edited by I. B. Alonso *et al.*, CERN, Geneva, Switzerland, Technical Report No. CERN-2020-010, 2020.
- [5] F. Willeke and J. Beebe-Wang, Electron ion collider conceptual design report, BNL, Upton, New York, Technical Report No. BNL-221006-2021-FORE, 2021.
- [6] A. Abada, M. Abbrescia, S. S. AbdusSalam *et al.*, FCC-hh: The Hadron Collider, *Eur. Phys. J. Special Topics* **228**, 755 (2019).
- [7] A. N. Lebedev, Longitudinal instability in the presence of an rf field, in *Proceedings of the 6th International Conference on High-Energy Accelerators, HEACC-1967, Cambridge, Massachusetts* (Cambridge Electron Accelerator, Cambridge, MA, 1967), pp. 284–288.
- [8] A. N. Lebedev, Coherent synchrotron oscillations in the presence of a space charge, *At. Energy* **25**, 851 (1968).
- [9] F. J. Sacherer, A longitudinal stability criterion for bunched beams, *IEEE Trans. Nucl. Sci.* **20**, 825 (1973).
- [10] A. G. Ruggiero and V. G. Vaccaro, Solution of the dispersion relation for longitudinal stability of an intense coasting beam in a circular accelerator (application to the ISR), CERN, Geneva, Technical Report No. CERN-ISR-TH-68-33, 1968.
- [11] J. M. Wang, Longitudinal symmetric coupled bunch modes, BNL, Upton, Technical Report No. BNL 51302, 1980.
- [12] Y. Chin, Longitudinal stability limit for electron bunches in a double rf system, *Nucl. Instrum. Methods Phys. Res.* **215**, 501 (1983).
- [13] K. Y. Ng, *Physics of Intensity Dependent Beam Instabilities* (World Scientific, Singapore, 2006).
- [14] A. W. Chao, M. Tigner, H. Weise, and F. Zimmermann, *Handbook of Accelerator Physics and Engineering*, 3rd ed. (World Scientific, Singapore, 2023).
- [15] V. I. Balbekov and S. V. Ivanov, Longitudinal beam instability threshold beam in proton synchrotrons, *At. Energy* **60**, 58 (1986).
- [16] R. R. Lindberg, Theory of coupled-bunch longitudinal instabilities in a storage ring for arbitrary rf potentials, *Phys. Rev. Accel. Beams* **21**, 124402 (2018).
- [17] A. Hofmann and F. Pedersen, Bunches with local elliptic energy distributions, *IEEE Trans. Nucl. Sci.* **26**, 3526 (1979).
- [18] V. I. Balbekov and S. V. Ivanov, The influence of chamber inductance on the threshold of longitudinal bunched beam instability, in *Proceedings of the 2nd European Particle Accelerator Conference, EPAC-1990, Nice, France* (JACoW, Geneva, Switzerland, 1990), pp. 1566–1568.
- [19] O. Boine-Frankenheim and T. Shukla, Space charge effects in bunches for different rf wave forms, *Phys. Rev. ST Accel. Beams* **8**, 034201 (2005).
- [20] O. Boine-Frankenheim and O. Chorniy, Stability of coherent synchrotron oscillations with space charge, *Phys. Rev. ST Accel. Beams* **10**, 104202 (2007).
- [21] A. Burov, Van Kampen modes for bunch longitudinal motion, in *Proceedings of the 46th ICFA Advanced Beam Dynamics Workshop on High-Intensity and High-Brightness Hadron Beams, HB-2010, Morschach, Switzerland* (JACoW, Geneva, Switzerland, 2010), arXiv: 1207.5826.
- [22] K. Oide and K. Yokoya, Longitudinal single bunch instability in electron storage rings, KEK, Tsukuba, Japan, Technical Report No. KEK-Preprint-90-10, 1990.
- [23] I. Karpov, T. Argyropoulos, and E. Shaposhnikova, Thresholds for loss of Landau damping in longitudinal plane, *Phys. Rev. Accel. Beams* **24**, 011002 (2021).
- [24] R. L. Gluckstern, Longitudinal impedance of a periodic structure at high frequency, *Phys. Rev. D* **39**, 2780 (1989).
- [25] S. A. Heifets and S. A. Kheifets, Coupling impedance in modern accelerators, *Rev. Mod. Phys.* **63**, 631 (1991).
- [26] M. Blaskiewicz, Longitudinal stability calculations, BNL, Upton, New York, Technical Report No. BNL-81969-2009-IR, 2009.
- [27] A. Burov, Longitudinal modes of bunched beams with weak space charge, *Phys. Rev. Accel. Beams* **24**, 064401 (2021).
- [28] A. W. Chao, *Physics of Collective Beam Instabilities in High Energy Accelerators* (Wiley, New York, 1993).

- [29] N. G. Van Kampen, On the theory of stationary waves in plasmas, *Physica (Utrecht)* **21**, 949 (1955).
- [30] N. G. Van Kampen, The dispersion equation for plasma waves, *Physica (Utrecht)* **23**, 641 (1957).
- [31] Y. H. Chin, K. Satoh, and K. Yokoya, Instability of a bunched beam with synchrotron frequency spread, *Part. Accel.* **13**, 45 (1983).
- [32] E. Shaposhnikova, Bunched beam transfer matrices in single and double rf systems, CERN, Geneva, Switzerland, Technical Report No. CERN-SL-94-19-RF, 1994.
- [33] I. Karpov, MELODY: Matrix Equations for Longitudinal beam Dynamics, <https://gitlab.cern.ch/ikarpov/melody>.
- [34] C. Y. Tan and A. Burov, Phase modulation of the bucket stops bunch oscillations at the Fermilab Tevatron, *Phys. Rev. ST Accel. Beams* **15**, 044401 (2012).
- [35] E. Shaposhnikova, T. Argyropoulos, P. Baudreghien, J. F. Esteban Muller, T. Mastoridis, G. Papotti, B. Salvant H. Timko, C. M. Bhat, and A. V. Burov, Flat bunches in the LHC, in *Proceedings of the 5th International Particle Accelerator Conference, IPAC-2014, Dresden, Germany (JACoW, Geneva, Switzerland, 2014)*, pp. 1413–1415.
- [36] I. Karpov and E. Shaposhnikova, Longitudinal coupled-bunch instability evaluation for FCC-hh, in *Proceedings of the 10th International Particle Accelerator Conference, IPAC-2019, Melbourne, Australia (JACoW, Geneva, Switzerland, 2019)*, pp. 297–300.
- [37] LHC injectors upgrade, Technical design report, Vol. I: Protons, Edited by J. Coupard, H. Damerau, A. Funken, R. Garoby, S. Gilardoni, B. Goddard, K. Hanke, A. Lombardi, D. Manglunki, M. Meddahi, B. Mikulec, G. Rumolo, E. Shaposhnikova, and M. Vretenar, CERN, Geneva, Switzerland, Technical Report No. CERN-ACC-2014-0337, 2014.
- [38] E. Shaposhnikova, Cures for beam instabilities in the CERN SPS and their limitations, in *Proceedings of the 39th ICFA Advanced Beam Dynamics Workshop on High Intensity High Brightness Hadron Beams, HB-2006, Tsukuba, Japan (CERN, Geneva, Switzerland, 2006)*, pp. 153–155.
- [39] E. Shaposhnikova, T. Argyropoulos, T. Bohl, C. Bhat, P. Baudreghien, A. Butterworth, T. Mastoridis, J. Muller, G. Papotti, J. Tuckmantel, and W. V. Delsolaro, Loss of Landau damping in the LHC, in *Proceedings of the 2nd International Particle Accelerator Conference, San Sebastián, Spain (EPS-AG, Spain, 2011)*, pp. 211–214.
- [40] G. Skripka, R. Nagaoka, M. Klein, F. Cullinan, and P. F. Tavares, Simultaneous computation of intrabunch and interbunch collective beam motions in storage rings, *Nucl. Instrum. Methods Phys. Res., Sect. A* **806**, 221 (2016).
- [41] K. Iliakis, H. Timko, S. Xydis, P. Tsapatsaris, and D. Soudris, Enabling large scale simulations for particle accelerators, *IEEE Trans. Parallel Distrib. Syst.* **33**, 4425 (2022).
- [42] H. Timko, S. Albright, T. Argyropoulos, H. Damerau, K. Iliakis, L. Intelisano, B. E. Karlsen-Baek, I. Karpov, A. Lasheen, L. Medina, D. Quartullo, J. Repond, A. L. Vanel, J. Esteban Müller, M. Schwarz, P. Tsapatsaris, and G. Typaldos, Beam longitudinal dynamics simulation studies, *Phys. Rev. Accel. Beams* **26**, 114602 (2023).
- [43] F. J. Sacherer, Bunch lengthening and microwave instability, *IEEE Trans. Nucl. Sci.* **24**, 1393 (1977).
- [44] I. Karpov, Longitudinal mode-coupling instabilities of proton bunches in the CERN Super Proton Synchrotron, *Phys. Rev. Accel. Beams* **26**, 014401 (2023).
- [45] S. Nese, Effective impedance for the threshold of loss of Landau damping, CERN, Geneva, Switzerland, Technical Report No. CERN-STUDENTS-Note-2021-214, 2021.
- [46] I. Karpov, T. Argyropoulos, S. Nese, and E. Shaposhnikova, New analytical criteria for loss of Landau damping in longitudinal plane, in *Proceedings of the 67th ICFA Advanced Beam Dynamics Workshop on High-Intensity and HighBrightness Hadron Beams, HB-2021, Batavia, IL (JACoW, Geneva, Switzerland, 2022)*, pp. 100–105.
- [47] L. Intelisano, H. Damerau, and I. Karpov, Longitudinal loss of Landau damping in the CERN Super Proton Synchrotron at 200 GeV, in *Proceedings of the 14th International Particle Accelerator Conference, IPAC-2023, Venice, Italy (JACoW, Geneva, Switzerland, 2023)*, pp. 2669–2672.
- [48] I. Karpov and E. Shaposhnikova, Impact of broadband impedance on longitudinal coupled-bunch instability threshold, in *Proceedings of the 13th International Particle Accelerator Conference, IPAC-2022, Bangkok, Thailand (JACoW, Geneva, Switzerland, 2022)*, pp. 2245–2248.
- [49] E. Shaposhnikova, Analysis of coupled bunch instability spectra, *AIP Conf. Proc.* **496**, 256 (1999).
- [50] CERN SPS longitudinal impedance model, <https://gitlab.cern.ch/longitudinal-impedance/SPS>.
- [51] A. Lasheen and E. Shaposhnikova, Evaluation of the CERN Super Proton Synchrotron longitudinal impedance from measurements of the quadrupole frequency shift, *Phys. Rev. Accel. Beams* **20**, 064401 (2017).